

A THEORETICAL PROOFS

A.1 PROOF OF THEOREM 1

Proof. Fix w_{ij} and set $f(\alpha) \equiv f_{ij}(\alpha) = g_{ij}(\alpha) = \partial \mathcal{L}(\alpha \Delta \mathbf{W}) / \partial w_{ij}$. By Eq. (4), $s_e(w_{ij}) = |w_{ij}| \left| \int_0^1 f(\alpha) d\alpha \right|$. Define the composite trapezoidal approximation and its sampled variant:

$$\mathcal{T}_N = \frac{1}{2N} \left[f(0) + 2 \sum_{k=1}^{N-1} f\left(\frac{k}{N}\right) + f(1) \right], \quad \tilde{\mathcal{T}}_M = \frac{1}{2N} [f(0) + 2(N-1) \bar{f}_M + f(1)], \quad (13)$$

where $\bar{f}_M = \frac{1}{M} \sum_{p=1}^M f(\alpha_p)$ with α_p i.i.d. drawn from the discrete uniform distribution on $\{1/N, \dots, (N-1)/N\}$.

Since $s_{agg}(w_{ij}) = |w_{ij}| |\tilde{\mathcal{T}}_M|$ and $\|x\| - \|y\| \leq |x - y|$, the triangle inequality yields

$$|s_e(w_{ij}) - s_{agg}(w_{ij})| \leq |w_{ij}| \left| \int_0^1 f - \tilde{\mathcal{T}}_M \right| \leq |w_{ij}| \left(\left| \int_0^1 f - \mathcal{T}_N \right| + |\mathcal{T}_N - \tilde{\mathcal{T}}_M| \right). \quad (14)$$

Step 1: discretization error. By assumption, f is twice continuously differentiable on $[0, 1]$ and $\sup_{\alpha \in [0, 1]} |f''(\alpha)| \leq C_2$. The standard error bound for the composite trapezoidal rule on $[0, 1]$ (see, e.g., classical numerical analysis texts) yields

$$\left| \int_0^1 f(\alpha) d\alpha - \mathcal{T}_N \right| \leq \frac{C_2}{12N^2}. \quad (15)$$

Step 2: sampling error. Let $\mu = \frac{1}{N-1} \sum_{k=1}^{N-1} f\left(\frac{k}{N}\right)$ denote the average of f over the $(N-1)$ interior nodes. A simple algebraic manipulation gives

$$|\mathcal{T}_N - \tilde{\mathcal{T}}_M| = \frac{1}{N} \left| \sum_{k=1}^{N-1} f\left(\frac{k}{N}\right) - (N-1) \bar{f}_M \right| = \frac{N-1}{N} |\mu - \bar{f}_M| \leq |\mu - \bar{f}_M|. \quad (16)$$

By assumption, $f(\alpha)$ is uniformly bounded on the discretization nodes, which is discussed in detail in Appendix B.1: there exists $B < \infty$ such that $|f(\alpha)| \leq B$ for all $\alpha \in \{1/N, \dots, (N-1)/N\}$. Therefore, each sample $f(\alpha_p)$ lies in $[-B, B]$, and Hoeffding's inequality for bounded random variables implies that, for any $\delta \in (0, 1)$,

$$\Pr(|\mu - \bar{f}_M| \geq t) \leq 2 \exp\left(-\frac{2Mt^2}{(2B)^2}\right) = 2 \exp\left(-\frac{Mt^2}{2B^2}\right). \quad (17)$$

Setting the right-hand side equal to δ and solving for t yields that, with probability at least $1 - \delta$,

$$|\mu - \bar{f}_M| \leq B \sqrt{\frac{2 \log(2/\delta)}{M}} \leq c B \sqrt{\frac{\log(1/\delta)}{M}} \quad (18)$$

for an absolute constant $c > 0$. Combining with the previous display gives

$$|\mathcal{T}_N - \tilde{\mathcal{T}}_M| \leq |\mu - \bar{f}_M| \leq c B \sqrt{\frac{\log(1/\delta)}{M}} \quad (19)$$

with probability at least $1 - \delta$.

Step 3: combining the bounds. Plugging Eq. (15) and Eq. (19) into the decomposition in Eq. (14) yields that, with probability at least $1 - \delta$,

$$|s_e(w_{ij}) - s_{agg}(w_{ij})| \leq |w_{ij}| \left(\frac{C_2}{12N^2} + c B \sqrt{\frac{\log(1/\delta)}{M}} \right), \quad (20)$$

which is exactly the claimed bound in Eq. (9). \square

A.2 HIGH-PROBABILITY STABILITY OF SNR_t

The resulting SNR-based score favors parameters with consistent, high-impact contributions and suppresses those with volatile or transient behavior. While the above formulation provides an intuitive interpretation of SNR, it remains essential to ensure its statistical stability with high probability, which is formally addressed in Theorem 2.

864 **Theorem 2.** Let $y_t = s_{agg}(w_{ij})$ be the per-epoch raw importance defined in Eq. (7). Since ϵ in
 865 Eq. (12) is a very small constant, it can be ignored. Therefore, we have:
 866

$$867 \quad \text{SNR}_t = \frac{\bar{s}_e^{(t)}}{\bar{U}^{(t)} + \epsilon} \approx \frac{\bar{s}_e^{(t)}}{\bar{U}^{(t)}}, \quad (21)$$

869 Assume that (y_t) is an i.i.d. sequence of sub-Gaussian random variables with mean μ and variance
 870 σ^2 , and let $d = \mathbb{E}[|y_t - \mu|] > 0$. For $\beta_1, \beta_2 \in (0, 1)$, define the effective EMA window lengths
 871

$$872 \quad n_{\text{eff}}(\beta_1) = \frac{1 + \beta_1}{1 - \beta_1}, \quad n_{\text{eff}}(\beta_2) = \frac{1 + \beta_2}{1 - \beta_2}, \quad n_{\text{eff}} = \min\{n_{\text{eff}}(\beta_1), n_{\text{eff}}(\beta_2)\}. \quad (22)$$

875 Then there exist universal constants $c_1, c_2, c_0 > 0$ such that, for any $\delta \in (0, 1)$ and all
 876

$$877 \quad t \geq t_{\text{burn}} = \left\lceil \frac{c_1}{1 - \min\{\beta_1, \beta_2\}} \log \frac{c_2}{\delta} \right\rceil, \quad (23)$$

879 the following holds with probability at least $1 - \delta$:

$$881 \quad |\text{SNR}_t - \mu/d| \leq C \sqrt{\frac{\log(2/\delta)}{n_{\text{eff}}}}, \quad C = \frac{2\sqrt{2}\sigma}{d} + 2c_0 \frac{\mu}{d^2} (\sigma + d). \quad (24)$$

884 *Proof.* We analyze the EMA under the stylized assumption stated in Theorem 2: (y_t) is an i.i.d.
 885 sub-Gaussian sequence with mean μ , variance proxy σ^2 , and $d = \mathbb{E}|y_t - \mu| > 0$.
 886

887 Recall that Eq. (10) and Eq. (11) define the EMAs

$$888 \quad \bar{s}_e^{(t)} = \beta_1 \bar{s}_{t-1} + (1 - \beta_1) y_t, \quad \bar{U}^{(t)} = \beta_2 \bar{U}_{t-1} + (1 - \beta_2) |y_t - \bar{s}_e^{(t)}|. \quad (25)$$

890 Unrolling the recursions (for t large enough so that transients are negligible) shows that
 891

$$892 \quad \bar{s}_e^{(t)} = \sum_{k \geq 0} w_k^{(1)} y_{t-k}, \quad w_k^{(1)} = (1 - \beta_1) \beta_1^k, \quad \bar{U}^{(t)} = (1 - \beta_2) \sum_{k \geq 0} \beta_2^k |y_{t-k} - \bar{s}_{t-k}|. \quad (26)$$

894 Note that $(w_k^{(1)})_{k \geq 0}$ is a geometric weight sequence with $\sum_k w_k^{(1)} = 1$ and
 895

$$896 \quad \|w^{(1)}\|_2^2 = \sum_{k \geq 0} (1 - \beta_1)^2 \beta_1^{2k} = \frac{1 - \beta_1}{1 + \beta_1} = \frac{1}{n_{\text{eff}}(\beta_1)}. \quad (27)$$

899 Below we write $n_{\text{eff}} = \min\{n_{\text{eff}}(\beta_1), n_{\text{eff}}(\beta_2)\}$.
 900

901 **Step 1: concentration of $\bar{s}_e^{(t)}$.** Since (y_t) are i.i.d. sub-Gaussian with mean μ and variance proxy
 902 σ^2 , any fixed weighted sum $\sum_k w_k^{(1)} y_{t-k}$ is also sub-Gaussian with mean μ and variance proxy
 903 $\sigma^2 \|w^{(1)}\|_2^2 = \sigma^2 / n_{\text{eff}}(\beta_1)$. Standard sub-Gaussian tail bounds then yield
 904

$$905 \quad \Pr\left(|\bar{s}_e^{(t)} - \mu| \geq \varepsilon\right) \leq 2 \exp\left(-\frac{c n_{\text{eff}}(\beta_1) \varepsilon^2}{\sigma^2}\right) \quad (28)$$

908 for an absolute constant $c > 0$. Setting the right-hand side to $\delta/2$ and solving for ε gives
 909

$$910 \quad |\bar{s}_e^{(t)} - \mu| \leq \sigma \sqrt{\frac{2 \log(4/\delta)}{n_{\text{eff}}(\beta_1)}} \leq \sqrt{2} \sigma \sqrt{\frac{\log(4/\delta)}{n_{\text{eff}}}} \quad (29)$$

913 with probability at least $1 - \delta/2$.
 914

915 **Step 2: concentration of $\bar{U}^{(t)}$.** We decompose $\bar{U}^{(t)}$ around $d = \mathbb{E}|y_t - \mu|$ as
 916

$$917 \quad |\bar{U}^{(t)} - d| \leq (1 - \beta_2) \left| \sum_{k \geq 0} \beta_2^k (|y_{t-k} - \mu| - d) \right| + (1 - \beta_2) \sum_{k \geq 0} \beta_2^k |y_{t-k} - \bar{s}_{t-k}| - |y_{t-k} - \mu|. \quad (30)$$

Define $X_t = |y_t - \mu| - d$, which is a centered, sub-exponential random variable whose tail parameters depend only on (σ, d) (because y_t is sub-Gaussian). Let $w_k^{(2)} = (1 - \beta_2)\beta_2^k$ denote the EMA weights for $\bar{U}^{(t)}$. Then $\sum_{k \geq 0} w_k^{(2)} = 1$ and

$$\|w^{(2)}\|_2^2 = \sum_{k \geq 0} (1 - \beta_2)^2 \beta_2^{2k} = \frac{1 - \beta_2}{1 + \beta_2} = \frac{1}{n_{\text{eff}}(\beta_2)}.$$

Applying a Bernstein-type concentration for weighted sums of i.i.d. sub-exponential variables (see, e.g., standard results on Orlicz norms) yields the existence of an absolute constant $c_0 > 0$ such that, for any $\delta \in (0, 1)$,

$$\Pr \left(\left| (1 - \beta_2) \sum_{k \geq 0} \beta_2^k X_{t-k} \right| \geq c_0(\sigma + d) \sqrt{\frac{\log(4/\delta)}{n_{\text{eff}}(\beta_2)}} \right) \leq \frac{\delta}{2}. \quad (31)$$

For the second term in Eq. (30), note that $\| |a - c| - |a - b| \| \leq |b - c|$ for any $a, b, c \in \mathbb{R}$, so

$$\| |y_{t-k} - \bar{s}_{t-k}| - |y_{t-k} - \mu| \| \leq \|\bar{s}_{t-k} - \mu\|.$$

Thus

$$(1 - \beta_2) \sum_{k \geq 0} \beta_2^k \| |y_{t-k} - \bar{s}_{t-k}| - |y_{t-k} - \mu| \| \leq (1 - \beta_2) \sum_{k \geq 0} \beta_2^k \|\bar{s}_{t-k} - \mu\|. \quad (32)$$

We now bound the right-hand side by splitting the sum into a recent window and its tail. Let

$$L = \left\lceil \frac{c_1}{1 - \beta_2} \log \frac{c_2}{\delta} \right\rceil \quad (33)$$

for absolute constants $c_1, c_2 > 0$ chosen large enough. For $t \geq L$, we have

$$(1 - \beta_2) \sum_{k \geq 0} \beta_2^k \|\bar{s}_{t-k} - \mu\| \leq (1 - \beta_2) \sum_{k=0}^L \beta_2^k \|\bar{s}_{t-k} - \mu\| + (1 - \beta_2) \sum_{k>L} \beta_2^k \|\bar{s}_{t-k} - \mu\|. \quad (34)$$

For the tail sum, $(1 - \beta_2) \sum_{k>L} \beta_2^k = \beta_2^{L+1}$ and, by choosing c_1, c_2 appropriately, we can ensure $\beta_2^{L+1} \leq \delta/(8c_2)$. For the finite window $\{t, t-1, \dots, t-L\}$, we apply Eq. (29) and a union bound over these $(L+1)$ indices to obtain, with probability at least $1 - \delta/2$,

$$|\bar{s}_{t-k} - \mu| \leq \sqrt{2} \sigma \sqrt{\frac{\log(4L/\delta)}{n_{\text{eff}}(\beta_1)}} \quad \text{for all } 0 \leq k \leq L. \quad (35)$$

Combining these bounds and using $n_{\text{eff}} \leq n_{\text{eff}}(\beta_1)$ yields

$$(1 - \beta_2) \sum_{k \geq 0} \beta_2^k \|\bar{s}_{t-k} - \mu\| \leq \tilde{c} \sigma \sqrt{\frac{\log(2/\delta)}{n_{\text{eff}}}} \quad (36)$$

with probability at least $1 - \delta/2$, for an absolute constant $\tilde{c} > 0$.

Putting Eq. (31) and Eq. (36) back into Eq. (30) and recalling that $n_{\text{eff}} \leq n_{\text{eff}}(\beta_2)$, we obtain that, for $t \geq t_{\text{burn}}$ and with probability at least $1 - \delta$,

$$|\bar{U}^{(t)} - d| \leq C'_2(\sigma + d) \sqrt{\frac{\log(2/\delta)}{n_{\text{eff}}}} \quad (37)$$

for an absolute constant $C'_2 > 0$. By increasing c_1 if necessary, we may ensure that the right-hand side in Eq. (37) is at most $d/2$, so that $\bar{U}^{(t)} \geq d/2$ holds on the same high-probability event.

972 **Step 3: bounding the ratio SNR_t .** On the event $\{\bar{U}^{(t)} \geq d/2\}$ we can control the ratio $\text{SNR}_t =$
 973 $\bar{s}_e^{(t)} / \bar{U}^{(t)}$ via the deterministic inequality
 974

$$975 \quad \left| \frac{\bar{s}_e^{(t)}}{\bar{U}^{(t)}} - \frac{\mu}{d} \right| \leq \frac{2}{d} |\bar{s}_e^{(t)} - \mu| + \frac{2\mu}{d^2} |\bar{U}^{(t)} - d|. \quad (38)$$

978 Combining Eq. (29) and Eq. (37) with Eq. (38), and noting that $n_{\text{eff}} \leq n_{\text{eff}}(\beta_1)$, gives
 979

$$980 \quad |\text{SNR}_t - \mu/d| \leq \left(\frac{2\sqrt{2}\sigma}{d} + 2c_0 \frac{\mu}{d^2} (\sigma + d) \right) \sqrt{\frac{\log(2/\delta)}{n_{\text{eff}}}} \quad (39)$$

984 with probability at least $1 - \delta$, for a suitable absolute constant $c_0 > 0$. This is exactly the claimed
 985 bound in Theorem 2 after setting $C = \frac{2\sqrt{2}\sigma}{d} + 2c_0 \frac{\mu}{d^2} (\sigma + d)$ and $t_{\text{burn}} = \lceil \frac{c_1}{1 - \min\{\beta_1, \beta_2\}} \log \frac{c_2}{\delta} \rceil$. \square
 986

987 B THE DISCUSSION OF THE ASSUMPTIONS IN THEOREM

989 B.1 THE ANALYSIS OF THE ASSUMPTION IN THEOREM 1

991 In this section, we focus on how the assumption in Theorem 1, that g_{ij} is twice continuously
 992 differentiable on the interval $[0, 1]$ with a bounded second derivative, leads to the conclusion that
 993 $g_{ij}(\alpha)$ is bounded. First, consider the following form of $g_{ij}(\alpha)$:

$$994 \quad g_{ij}(\alpha) = \frac{\partial \mathcal{L}(\alpha \Delta \mathbf{W})}{\partial w_{ij}}, \quad \alpha \in [0, 1], \quad (40)$$

997 The analysis of Theorem 1 relies solely on the assumption that g_{ij} is twice differentiable on the
 998 interval $[0, 1]$ and that its second derivative is bounded, which allows the application of the composite
 999 trapezoidal rule, leading to a discretization error of $\mathcal{O}(N^{-2})$. Specifically, numerical analysis
 1000 typically assumes the existence of a constant $C_2 < \infty$ such that:

$$1002 \quad \sup_{\alpha \in [0, 1]} |g_{ij}''(\alpha)| \leq C_2. \quad (41)$$

1004 Under this assumption, we can derive the following error bound:
 1005

$$1006 \quad \left| \int_0^1 g_{ij}(\alpha) d\alpha - \mathcal{T}_N \right| \leq \frac{C_2}{12N^2}, \quad (42)$$

1009 This equation provides the theoretical basis for the $\mathcal{O}(N^{-2})$ discretization error term in Theorem 1.
 1010 This requirement is essentially a standard smoothness assumption in trapezoidal integration and does
 1011 not involve any specific distributional assumptions. Furthermore, the condition of bounded second
 1012 derivatives directly implies that g_{ij} itself is bounded. By the fundamental theorem of calculus:

$$1014 \quad g_{ij}'(\alpha) = g_{ij}'(0) + \int_0^\alpha g_{ij}''(t) dt, \quad g_{ij}(\alpha) = g_{ij}(0) + \int_0^\alpha g_{ij}'(t) dt, \quad (43)$$

1016 We can obtain the bound for all $\alpha \in [0, 1]$:

$$1018 \quad |g_{ij}'(\alpha)| \leq |g_{ij}'(0)| + \int_0^1 |g_{ij}''(t)| dt \leq |g_{ij}'(0)| + C_2, \quad (44)$$

1021 Thus,

$$1022 \quad |g_{ij}(\alpha)| \leq |g_{ij}(0)| + \int_0^1 |g_{ij}'(t)| dt \leq |g_{ij}(0)| + |g_{ij}'(0)| + C_2 \triangleq B. \quad (45)$$

1024 This implies that $g_{ij}(\alpha)$ is bounded on $[0, 1]$. When we sample α from the finite set $\{1/N, \dots, (N-1)/N\}$, the resulting random variable $g_{ij}(\alpha)$ is bounded by constant B .

1026 B.2 THE ANALYSIS OF THE I.I.D. ASSUMPTION IN THEOREM 2
10271028 Theorem 2 assumes that the per-epoch raw scores $y_t = s_{agg}(w_{ij})$ form an i.i.d. sub-Gaussian
1029 sequence with a common mean μ and variance σ^2 . However, strictly speaking, y_t depends on the
1030 current model parameters $\mathbf{W}^{(t)}$, which are updated across epochs, so exact i.i.d. is an idealization.
10311032 Our goal is to model the regime in which the training dynamics have *stabilized*: after an initial
1033 transient phase (discarded via the burn-in time t_{burn}), the statistics of the gradient noise around the
1034 current solution change only slowly. Furthermore, within the effective EMA window $n_{\text{eff}}(\beta_1, \beta_2)$,
1035 the gradient sequence can be approximated as having nearly stationary mean and variance. In this
1036 regime, standard extensions of EMA concentration results to weakly dependent or mixing sequences
1037 apply. We chose the i.i.d. setting for clarity of presentation and to keep the notation simple. It is
1038 important to note that Theorem 2 is derived under this stylized, locally stationary noise assumption,
1039 and is meant to provide intuition about how the EMA window size and variance control the stability
1040 of SNR_t , rather than to capture every aspect of LLM training dynamics exactly.
10411042 To support this approximation empirically, we provide a small diagnostic in Appendix G: for a
1043 representative layer on BoolQ, we plot the time series of y_t and its running mean/variance across
1044 epochs. We observe that, after the early epochs, both the mean and variance of y_t quickly settle into a
1045 narrow band, and the lag-1 autocorrelation becomes small. Correspondingly, the SNR_t curves are
1046 nearly flat after burn-in. These observations suggest that, in the regime where EMA-based importance
1047 is actually used for rank pruning, the i.i.d./local stationarity approximation is reasonably accurate.
10481049 Finally, we emphasize that these assumptions are used only in our theoretical analysis; the algorithm
1050 itself does not rely on them. Even when the exact assumptions are relaxed, the qualitative conclusions
1051 remain the same: (i) our IG estimator trades off discretization error $O(N^{-2})$ and sampling error
1052 $O(M^{-1/2})$, and (ii) EMA-based SNR_t scores become more stable as the effective sample size
1053 increases and the process enters a locally stationary regime.
10541055 C HYPERPARAMETER SETTINGS
10561057 During the training process, we tune the learning rate from $\{5 \times 10^{-4}, 1 \times 10^{-4}, 5 \times 10^{-4}, 1 \times$
1058 $10^{-3}, 2 \times 10^{-4}\}$ and pick the best learning rate for every method. For the MNLI, QNLI, and QQP, we
1059 set the batch size to 128. For RTE, MRPC, CoLA, and STS-B, the batch size is set to 32. For SST-2,
1060 we use a batch size of 64. For all other tasks, the batch size is set to 16. All baseline methods follow
1061 the same settings as IGU-LoRA, as detailed in Table 6. In IGU-LoRA, several key hyperparameters
1062 $\epsilon, M, N, \beta_1, \beta_2$ are set to $1 \times 10^{-6}, 16, 20, 0.85$, and 0.85 , respectively, as detailed in Table 7. They
1063 remain constant throughout the experiment, and their sensitivity is discussed in the main text.
10641065 **Table 6:** Hyperparameter setup of IGU-LoRA for training on different datasets.

Dataset	learning rate	batch size	Max. Sequence Length	# epochs	γ	t_i	Δ_T	t_f
MNLI	5×10^{-4}	128	512	25	0.1	500	20	10000
RTE	1×10^{-3}	32	512	25	0.1	300	5	2500
QNLI	5×10^{-4}	128	512	25	0.1	400	20	10000
MRPC	1×10^{-3}	32	512	25	0.1	300	5	2500
QQP	5×10^{-4}	128	512	25	0.1	500	20	10000
SST-2	1×10^{-3}	64	512	25	0.1	400	20	5000
CoLA	1×10^{-3}	32	512	25	0.1	300	5	2500
STS-B	2×10^{-3}	32	512	25	0.1	300	5	2500
BoolQ	5×10^{-4}	16	512	25	0.1	500	20	10000
ARC-e	5×10^{-4}	16	512	25	0.1	500	20	10000
ARC-c	5×10^{-4}	16	512	25	0.1	500	20	10000
COPA	1×10^{-3}	16	512	25	0.1	500	20	10000
AQuA	1×10^{-4}	16	512	25	0.1	500	20	10000
MMLU	1×10^{-4}	128	512	15	0.1	500	20	10000
VQA	2×10^{-4}	32	512	25	0.1	300	20	10000
GAQ	5×10^{-4}	32	512	25	0.1	300	20	10000
MVLR ²	5×10^{-4}	32	512	25	0.1	300	20	10000
COCO	2×10^{-4}	32	512	25	0.1	300	20	10000

1080
1081
1082
1083
1084
1085
1086
1087
1088
1089
1090
1091
1092
1093
1094
1095
1096
1097
1098
1099
1100
1101
1102
Table 7: Setting of the 5 hyperparameters ($\epsilon, M, N, \beta_1, \beta_2$) in IGU-LoRA.

Hyperparameter	ϵ	M	N	β_1	β_2
Value	1×10^{-6}	16	20	0.85	0.85

D ABLATION STUDY ON HIGH-IMPACT PARAMETERS

To further validate the effectiveness of IGU-LoRA in identifying high-impact parameters, we conduct an ablation study on high-impact parameters. Specifically, we remove the high-rank and low-rank modules with the highest IGU-LoRA scores from different layers of the Qwen2.5-0.5B model and evaluate the performance drop on the Boolq and GSM8K datasets. As shown in Table 8, removing the high-rank modules from the K module in Layer 3 (L3_K) and the V module in Layer 10 (L10_V) results in a performance drop of 1.30 and 1.33 points on Boolq, respectively. Similarly, removing the high-rank modules from the Q module in Layer 22 (L22_Q) and the K module in Layer 17 (L17_K) results in performance drops of 1.80 and 1.73 points on GSM8K, respectively. In contrast, removing the low-rank modules from the K module in Layer 1 (L1_K) and the V module in Layer 3 (L3_V) results in only minor performance drops of 0.05 and 0.10 points on Boolq, respectively. The same trend is observed on GSM8K when removing the low-rank modules from the Q module in Layer 8 (L8_Q) and the K module in Layer 6 (L6_K), resulting in performance drops of 0.11 and 0.15 points, respectively. These results demonstrate that IGU-LoRA effectively identifies high-impact parameters, as their removal leads to significant performance degradation compared to low-impact parameters.

Table 8: Ablation study on the impact of removing high-rank and low-rank modules from different layers on Qwen2.5-0.5B model performance. The numbers in parentheses indicate the performance drop compared to the model with no modules removed. The left table and the right table represent results on Boolq and GSM8K, respectively.

	Module Removed	Rank	Boolq		Module Removed	Rank	GSM8K
1	L3_K	10	81.15 (-1.30)	1	L22_Q	12	32.35 (-1.80)
2	L10_V	10	81.12 (-1.33)	2	L17_K	11	32.42 (-1.73)
3	L3_K / L10_V	10 / 10	80.44 (-2.01)	3	L22_Q / L17_K	12 / 11	31.15 (-3.00)
4	L1_K	5	82.40 (-0.05)	4	L8_Q	6	34.05 (-0.11)
5	L3_V	5	82.35 (-0.10)	5	L6_K	6	34.01 (-0.15)
6	L1_K / L3_V	5 / 5	82.30 (-0.15)	6	L8_Q / L6_K	6 / 6	33.84 (-0.32)
7	-	-	82.45	7	-	-	34.16

E GENERALIZATION SUPPLEMENTARY EXPERIMENTS

To further validate the generalization performance of IGU-LoRA, we conduct additional experiments on the MMLU benchmark using the Llama2-7B model. As shown in Table 9, IGU-LoRA achieves an average accuracy of 51.07%, which is very close to the full fine-tuning method (51.54%) and outperforms LoRA (49.94%). Notably, IGU-LoRA demonstrates superior performance in Science, Technology, Engineering, and Mathematics (STEM) and Social Science subjects, achieving accuracies of 41.71% and 58.12%, respectively. These results further confirm the effectiveness of IGU-LoRA in enhancing the generalization capabilities of fine-tuned models across diverse subject areas.

Table 9: The generalization performance of fine-tuning the Llama2-7B model on the MMLU benchmark using different methods, reporting the average results over 5 random seeds.

Method	Humanities	STEM	Social.	Other	Avg.
Full FT	49.91	41.70	57.53	57.02	51.54
LoRA	46.15	40.84	56.63	56.23	49.94
IGU-LoRA	<u>47.33</u>	41.71	58.12	57.10	<u>51.07</u>

F MULTIMODAL BENCHMARK SUPPLEMENTARY EXPERIMENTS

To further demonstrate the effectiveness of IGU-LoRA in multimodal tasks, we conduct additional experiments on the VQAv2, GAQ, NVR² and COCO Captioning datasets using the VL-BART (Su et al., 2019). As shown in Table 10, IGU-LoRA achieves an average score of 77.47, outperforming

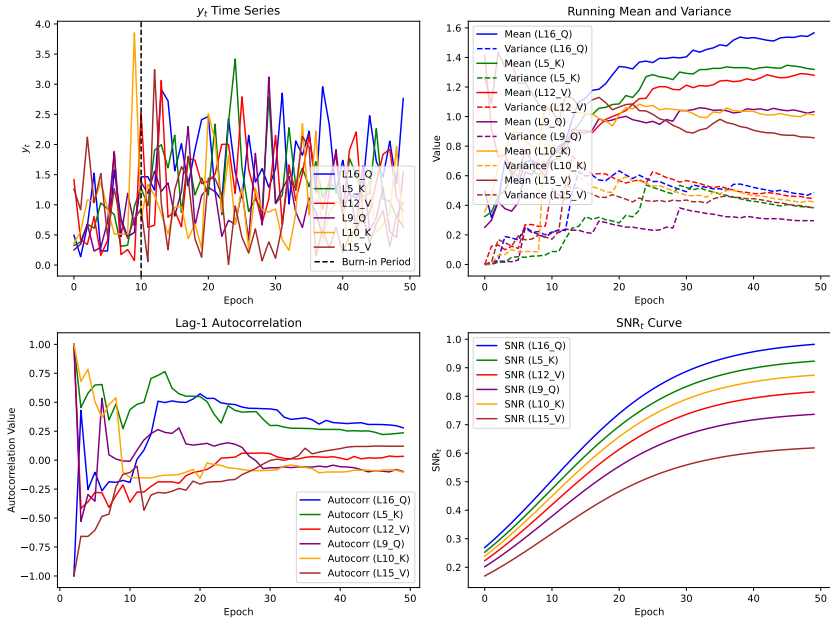
1134 LoRA (74.31) and DoRA (77.40), and closely approaching the performance of full fine-tuning
 1135 (77.35). These results further validate the capability of IGU-LoRA to effectively adapt multimodal
 1136 models while maintaining high performance across different tasks.

1137 **Table 10:** Performance comparison of different fine-tuning methods on the VQA, GAQ, NVLR² and COCO
 1138 datasets using the VL-BART model. The results are averaged over 5 random seeds.

Method	VQAv2	GAQ	NVLR ²	COCO Captioning	Avg.
Full FT	66.91	56.72	73.71	112.04	77.35
LoRA	64.32	54.10	71.25	109.56	74.31
DoRA	65.81	54.71	73.14	115.93	77.40
IGU-LoRA	65.78	55.32	73.42	115.36	77.47

G THE VERIFICATION OF THE I.I.D./LOCAL STATIONARITY APPROXIMATION IN THEOREM 2.

1150 To validate the i.i.d. / local stationarity approximation used in Theorem 2, we conduct an empirical
 1151 analysis of the importance score statistics during the fine-tuning process. Specifically, we monitor
 1152 several representative modules (e.g., the L16.Q module for the 16-th layer’s Q component and the
 1153 L5.K module for the 5-th layer’s K component) across multiple training iterations on the BoolQ
 1154 dataset. We observe that, after the initial epochs, the mean and variance of y_t quickly stabilize
 1155 within a narrow range, and the first-order lag autocorrelation becomes very small. Correspondingly,
 1156 the SNR_t curve becomes nearly flat after the burn-in period. These observations suggest that the
 1157 i.i.d./local stationarity approximation is reasonable and accurate during the stage when EMA-based
 1158 importance-ranking pruning is applied in practice.



1179 **Figure 7:** Empirical analysis of importance score statistics during fine-tuning. The plots show the changes
 1180 in y_t , the mean and variance of y_t , the first-order lag autocorrelation, and SNR_t across training iterations for
 1181 representative module parameters.

H EFFECTS OF SAMPLE ORDER AND BATCH SIZE

1186 To investigate the effects of sample order and batch size on the performance of IGU-LoRA, we conduct
 1187 experiments using the Qwen-2.5-0.5B model on the BoolQ dataset. The results are summarized as
 1188 follows:

1188
 1189 **Sample Order / Random Seed.** we trained with a fixed batch size using five different random
 1190 seeds. These seeds control the data shuffling and the sampled integration nodes α_k . The downstream
 1191 accuracy varies slightly across seeds (within Δ_{acc} absolute points, indicating a small change), which
 1192 demonstrates that the sample order has high stability on the results.

1193 **Batch Size.** We further vary the batch size (e.g., 2, 4, 8, 16, 32) while keeping all other hyperparameters
 1194 fixed. The resulting test accuracy again shows only minor variation. This proves that batch size
 1195 does not have a significant impact on the results. The detailed results are presented in Table 11.

1196 **Table 11: Effect of Batch Size on BoolQ Accuracy across Different Random Seeds**

1197 Batch Size	1198 Seed 1	1199 Seed 2	1200 Seed 3	1201 Seed 4	1202 Seed 5
1203 2	1204 82.46	1205 82.47	1206 82.45	1207 82.46	1208 82.45
1209 4	1210 82.45	1211 82.46	1212 82.44	1213 82.45	1214 82.44
1215 8	1216 82.44	1217 82.45	1218 82.43	1219 82.44	1220 82.43
1221 16	1222 82.45	1223 82.46	1224 82.44	1225 82.45	1226 82.44
1227 32	1228 82.40	1229 82.41	1230 82.39	1231 82.40	1232 82.39

1204 I DATASETS AND METRICS

1205 I.1 GLUE BENCHMARK TASKS

1206 **Single-sentence Classification Tasks.** (1) *CoLA (Corpus of Linguistic Acceptability)*: Determine
 1207 whether a sentence adheres to grammatical rules (binary classification). (2) *SST-2 (Stanford Sentiment
 1208 Treebank)*: Movie review sentiment analysis (positive/negative binary classification).

1209 **Sentence-pair Classification Tasks.** (1) *MRPC (Microsoft Research Paraphrase Corpus)*: Determine
 1210 whether two sentences are semantically equivalent (binary classification). (2) *QQP (Quora Question
 1211 Pairs)*: Determine whether two Quora questions are semantically identical (binary classification).
 1212 (3) *RTE (Recognizing Textual Entailment)*: Determine whether a sentence pair entails a relationship
 1213 (three-class classification: entailment/contradiction/neutral).

1214 **Similarity and Regression Task.** *STS-B (Semantic Textual Similarity Benchmark)*: Calculate the
 1215 semantic similarity between two sentences (continuous value from 1 to 5).

1216 **Question-answering Task.** *QNLI (Question-answering NLI)*: Determine whether a sentence contains
 1217 the answer to a given question (binary classification).

1218 **Natural Language Inference Task.** *MNLI (Multi-Genre Natural Language Inference)*: Large-scale
 1219 cross-domain textual entailment classification (three-class classification).

1220 I.2 MATHEMATICAL AND COMMON-SENSE REASONING TASKS

1221 **Mathematical Reasoning Tasks.** (1) *AQuA (Algebra question answering)*: Derive the correct answer
 1222 from a given algebraic problem (multiple-choice) and generate the corresponding solution process
 1223 (Rationales). (2) *GSM8K (Grade school math 8K)*: Perform multi-step reasoning on mathematical
 1224 problems described in natural language.

1225 **Common-Sense Reasoning Tasks.** (1) *BoolQ (Boolean questions)*: Determine whether the answer
 1226 to a given question, based on the provided paragraph, is "Yes" (True) or "No" (False). (2) *ARC-e
 1227 (AI2 reasoning challenge - easy)*: Select the most reasonable answer from a given set of scientific
 1228 questions (Multiple-choice question). (3) *ARC-c (AI2 reasoning challenge - challenge)*: Combine
 1229 multi-step reasoning and cross-domain knowledge to provide answers. (4) *COPA (Choice of plausible
 1230 alternatives)*: Select the most plausible cause or effect for a given premise from two provided
 1231 alternatives. The task requires understanding of causal relationships and commonsense reasoning in
 1232 everyday scenarios.

1233 I.3 MULTIMODAL BENCHMARK TASKS

1234 **Visual Question Answering Tasks.** (1) *VQAv2 (Visual Question Answering v2)*: Given an image and
 1235 a related question, select the most appropriate answer from multiple choices. (2) *GAQ (Generalized*

1242 *Question Answering*). This task extends VQA to a more generalized setting, where the model is asked
 1243 to answer a wider range of questions based on visual context.

1244 **Visual-Linguistic Reasoning Task.** (1) *NLVR2 (Natural Language for Visual Reasoning 2)*. Given a
 1245 pair of images and a natural language statement, determine whether the statement accurately describes
 1246 the relationship between the two images.

1247 **Image Captioning Task.** (1) *COCO Captioning*. Generate descriptive captions for images in the
 1248 COCO dataset, evaluating the model’s ability to understand and describe visual content accurately.

1249 **Table 12:** Summary of the benchmark datasets.

1251 Datasets	1251 # train	1251 # dev	1251 # test	1251 Type	1251 Metrics
Common-Sense reasoning tasks					
1254 BoolQ	1254 9427	1254 -	1254 3270	1254 Common-Sense reasoning	1254 Acc
1255 ARC-e	1255 2251	1255 570	1255 2376	1255 Common-Sense reasoning	1255 Acc
1256 ARC-c	1256 1119	1256 299	1256 1172	1256 Common-Sense reasoning	1256 Acc
1257 COPA	1257 400	1257 100	1257 500	1257 Common-Sense reasoning	1257 Acc
Mathematical reasoning tasks					
1259 AQuA	1259 97467	1259 254	1259 254	1259 Mathematical reasoning	1259 Acc
1260 GSM8K	1260 7473	1260 -	1260 1319	1260 Mathematical reasoning	1260 Acc
GLUE benchmark tasks					
1263 SST-2	1263 67k	1263 872	1263 1.8k	1263 Sentiment	1263 Acc
1264 MNLI	1264 393k	1264 20k	1264 20k	1264 NLU	1264 Acc
1265 QQP	1265 364k	1265 40k	1265 391k	1265 Paraphrase	1265 Acc-F1
1266 MRPC	1266 3.7k	1266 408	1266 107k	1266 Paraphrase	1266 Acc-F1
1267 RTE	1267 2.5k	1267 176	1267 3k	1267 NLU	1267 Acc
1268 QNLI	1268 108k	1268 5.7k	1268 5.7k	1268 QA/NLI	1268 Acc
1269 CoLA	1269 8.5k	1269 1k	1269 1k	1269 Acceptability	1269 Mcc
1270 STS-B	1270 7k	1270 1.5k	1270 1.4k	1270 Similarity	1270 Corr

I.4 DATASET STATISTICS

1274 In our experiments, we compare performance across multiple tasks, including the GLUE benchmark,
 1275 which consists of eight datasets: CoLA, SST-2, MRPC, QQP, STS-B, MNLI, QNLI, and RTE; three
 1276 common-sense reasoning tasks (BoolQ, ARC-e, and ARC-c); and two mathematical reasoning tasks
 1277 (AQuA and GSM8K). The dataset statistics are presented in Table 12.

I.5 EVALUATION METRICS

1281 As shown in Table 12, we strictly follow the official settings of GLUE and use the same metrics
 1282 as Wang et al. (2018). For MNLI, we report the average of the accuracy scores on the matched and
 1283 mismatched test sets. For MRPC and QQP, we report Acc-F1, the average accuracy, and F1 scores.
 1284 For STS-B, we report Corr, which denotes the average of the Pearson and Spearman correlation
 1285 coefficients. For CoLA, we report Mcc, which is the Matthews correlation. For all other tasks,
 1286 we report accuracy (Acc). Since the common sense and math reasoning tasks usually come with a
 1287 definite answer choice, we will directly consider the correctness of the final answers. Thus, we report
 1288 accuracy (denoted as Acc).

J BASELINE DETAILS

- 1292 • *Full fine-tuning* is the most common approach for adaptation. During fine-tuning, the model is
 1293 initialized with pre-trained weights and biases, and all model parameters undergo gradient updates.
- 1294 • *LoRA* (Hu et al., 2022a) is a representative parameter-efficient fine-tuning (PEFT) method. It
 1295 introduces two low-rank matrices to parameterize the incremental weight updates, and only these
 1296 lightweight components are updated during fine-tuning. The number of trainable parameters is

1296 determined by the rank r and the number of inserted adaptation matrices n , allowing for fine-grained
 1297 control over the adaptation budget.

1298 • *AdaLoRA* (Zhang et al., 2023) extends the conventional LoRA framework by introducing a dy-
 1299 namic rank adaptation mechanism. It parameterizes the low-rank adapters using singular value
 1300 decomposition (SVD), and evaluates the importance of each parameter based on the magnitude of its
 1301 corresponding singular value. This importance score then guides a progressive rank pruning process,
 1302 allowing the model to dynamically reallocate its limited parameter budget to more critical layers or
 1303 modules.

1304 • *DoRA* (Liu et al., 2024b) enhances the learning capacity and adaptability of pretrained models by
 1305 decoupling weight matrices into two distinct components: magnitude and direction. The key idea is to
 1306 keep the magnitude fixed and apply LoRA-style low-rank updates only to the directional component.
 1307 This separation allows for more expressive and geometry-aware adaptation while preserving the norm
 1308 of the original weights, which helps stabilize training and maintain alignment with the pretrained
 1309 model. Since only the direction is modified, DoRA introduces no additional inference overhead,
 1310 making it efficient and scalable for deployment.

1311 • *AutoLoRA* (Xu et al., 2023) is a meta-learning-based fine-tuning approach designed to automatically
 1312 determine the optimal rank for each layer in Low-Rank Adaptation (LoRA). It introduces a learnable
 1313 selection variable for each rank-1 matrix and dynamically adjusts these variables using a meta-
 1314 learning strategy. By jointly optimizing the rank configuration along with the LoRA parameters,
 1315 AutoLoRA significantly improves fine-tuning efficiency and overall performance.

1316 • *Adapter* (Houlsby et al., 2019) inserts lightweight bottleneck modules between each layer of the
 1317 pretrained model, updating only these newly introduced modules during fine-tuning while keeping
 1318 the original model parameters frozen.

1319 • *P-tuning v2* (Liu et al., 2021) is an improved prompt tuning method that inserts trainable prompt
 1320 tokens at the input layer and across multiple model layers. This design increases the trainable
 1321 parameters from approximately 0.01% to 0.1%-3% of the full model, while maintaining parameter
 1322 efficiency. P-tuning v2 enhances optimization stability and improves performance across various
 1323 tasks by integrating task-specific information deeper into the model.

1324 • *(IA)³* (Liu et al., 2022a) introduces learnable scaling vectors at key locations in the Transformer
 1325 architecture, such as the keys and values in the self-attention mechanism and the intermediate
 1326 activations in the feed-forward networks. These vectors are applied via element-wise multiplication to
 1327 modulate the internal activations, enabling flexible control over the model’s output without modifying
 1328 the original model parameters.

1329 • *SSP* (Hu et al., 2022b) leverages structural sparsity to guide the automatic search for parameter
 1330 insertion locations, activating trainable parameters only in the most important substructures. This
 1331 enables higher efficiency without sacrificing model performance.

1332 • *GoRA* (He et al., 2025) leverages gradient-driven adaptive low-rank adjustment to dynamically
 1333 adjust the rank of low-rank adaptation layers during training. By using gradient information, GoRA
 1334 ensures that the model can allocate computational resources more efficiently, adjusting the rank
 1335 based on the importance of each layer for different tasks and training stages. This method maintains
 1336 computational efficiency while improving model performance, adapting the low-rank configuration
 1337 to meet the specific needs of the training process.

K ADDITIONAL RELATED WORKS

K.1 DYNAMIC RANK ALLOCATION

1343 Dynamic rank allocation gains increasing attention in deep learning model optimization, with various
 1344 methods proposed to improve adaptability and efficiency. Several other notable approaches are intro-
 1345 duced beyond AdaLoRA (Zhang et al., 2023) and AutoLoRA (Xu et al., 2023). LoSA (Huang et al.,
 1346 2025) integrates sparsity and low-rank adaptation, dynamically adjusting both using representation
 1347 mutual information and reconstruction error. PRILoRA (Benedek & Wolf, 2024) employs a heuristic
 1348 strategy that linearly increases ranks from lower to higher layers, motivated by the observation that
 1349 higher layers often require greater adaptability in transfer learning. ALoRA (Liu et al., 2024c) further
 incorporates a novel mechanism, AB-LoRA, which assesses the importance of individual LoRA

1350 ranks and incrementally prunes redundant components, reallocating the freed budget to more critical
1351 Transformer modules. These methods provide diverse rank allocation strategies that contribute to
1352 more efficient fine-tuning of large models.
1353

1354 L THE USE OF LARGE LANGUAGE MODELS 1355

1356 During the preparation of this manuscript, large language models (LLMs) were employed in several
1357 auxiliary capacities. First, at the writing stage, LLMs were utilized to refine and translate the text,
1358 thereby enhancing the overall fluency, readability, and precision of academic expression. Second,
1359 in relation to experiments and results presentation, LLMs assisted in generating parts of the code
1360 for data visualization and figure plotting, which facilitated a more efficient presentation of research
1361 findings. Third, in surveying the research landscape and related work, LLMs provided support for
1362 literature searches, helping us to locate and summarize relevant studies in the field systematically.
1363 Finally, in the theoretical component of this work, LLMs offered auxiliary support in structuring
1364 complex proofs and verifying critical derivation steps, contributing to the clarity and rigor of our
1365 theoretical analysis. It should be emphasized that all uses of LLMs were strictly auxiliary in nature;
1366 the formulation of research questions, the design of methods, the core theoretical derivations, and the
1367 experimental analyses were all carried out independently by the authors.
1368
1369
1370
1371
1372
1373
1374
1375
1376
1377
1378
1379
1380
1381
1382
1383
1384
1385
1386
1387
1388
1389
1390
1391
1392
1393
1394
1395
1396
1397
1398
1399
1400
1401
1402
1403